RSC Advances

PAPER

View Article Online
View Journal | View Issue

Cite this: *RSC Adv.*, 2024, **14**, 7229

Improvement of the rate capability of all-solid-state cells with Fe-based polysulfide positive electrode materials by modifying the microstructure†

Tomonari Takeuchi, *[a] Noboru Taguchi, [a] Mitsunori Kitta, [a] Toyonari Yaji, [b] Misae Otoyama, [a] Kentaro Kuratani [a] and Hikari Sakaebe [ac]

Received 18th December 2023
Accepted 15th February 2024

DOI: 10.1039/d3ra08641k

rsc.li/rsc-advances

We successfully prepared an Fe- and Li-containing polysulfide positive electrode material (Li_8FeS_5–Li_2FeS_2 composite) that shows a high specific capacity (>500 mA h g^{-1}) with improved rate capability in all-solid-state cells. High-resolution TEM analysis indicated the coexistence of small crystallites of high-conductivity Li_2FeS_2 and FeS, as well as low-crystallinity Li_2S, in the composite, and this microstructure is responsible for the improved battery performance.

Introduction

Recently, there has been an increasing demand for high-energy storage systems, particularly those applicable in electric vehicles. Currently, next-generation batteries are required with a much higher energy density than that of the conventional lithium-ion batteries consisting of oxide-based cathode materials (practically *ca.* 200 W h kg^{-1}).[1,2] To date, several candidates such as lithium–oxygen batteries (theoretically *ca.* 3500 W h kg^{-1}),[3,4] lithium–sulphur (Li–S) batteries (*ca.* 2600 W h kg^{-1}),[5] and Zn–oxygen batteries (*ca.* 1100 W h kg^{-1})[6] have been included in next-generation batteries. Among them, the Li–S battery is a promising system that generates high energy density in a closed system (without introducing gaseous components).

Lithium sulphide (Li_2S) is a potential cathode active material in Li–S cells with a high theoretical capacity (*ca.* 1170 mA h g^{-1}) and has the advantage that a variety of anode materials such as graphite and silicon can be used in practical battery systems.[7–13] However, Li_2S shows high electrical resistivity, which gives rise to poor material usage in the cells. In order to enhance the conductivity of Li_2S, several attempts such as forming composites with carbon (Li_2S–C)[10–12] or metals (Li_2S–Fe, Li_2S–Cu, and Li_2S–V)[7–9] have been made. Along with the latter material design, we developed the Fe-containing polysulfide material Li_xFeS_y, which showed a relatively high specific capacity of *ca.* 730 mA h g^{-1} for the Li_8FeS_5 cell with a non-aqueous liquid electrolyte.[9] However, these Li_xFeS_y cells showed capacity degradation with cycling, as observed often for Li–S cells with a liquid electrolyte, partly because of the side reactions between the sulphide electrode material and the liquid electrolyte and partly because of the dissolution of polysulfides formed during electrochemical charge/discharge reactions into the liquid electrolyte. Replacing the liquid electrolyte with the solid electrolyte is a promising approach to solve these problems, and there have been many reports on all-solid-state cells with metal polysulfide cathode materials such as Li_2TiS_3, Li_3NbS_4, and Li_3CuS_2, showing superior electrochemical performances.[14–16] Much recently, V-containing polysulfide materials (Li_xVS_y) have been developed, and their all-solid-state cells showed superior rate capability with a higher specific capacity (>600 mA h g^{-1}), which originated from its higher electrical conductivity (>10^{-2} S cm^{-1}).[17]

In this study, we prepared an Fe-based polysulfide electrode material (Li_xFeS_y) in an attempt to show superior rate capability with high specific capacity in all-solid-state cells. Fe-based electrode materials are advantageous from the standpoints of resource abundance and cost, which would be beneficial for application to batteries, particularly in electric vehicles. However, Li_xFeS_y showed a relatively low conductivity of *ca.* 1.0 × 10^{-5} S cm^{-1} for Li_8FeS_5, implying a necessity for improvement in performance, particularly in rate capability. The lower conductivity of Li_8FeS_5 so far (denoted as Li_8FeS_5-H sample) is partly due to the rather homogeneous component originating from the preparation process of both heating and milling. We prepared "inhomogeneous" Li_8FeS_5, that is, coexisting with some high-conductivity components such as FeS and Li_2FeS_2 by "incomplete" milling of Li_2S and FeS (denoted as Li_8FeS_5-MM

[a]*National Institute of Advanced Industrial Science and Technology (AIST), Midorigaoka 1-8-31, Ikeda, Osaka 563-8577, Japan. E-mail: takeuchi.tomonari@aist.go.jp*

[b]*Synchrotron Radiation Center, Ritsumeikan University, Kusatsu, Shiga 525-8577, Japan*

[c]*Kyushu University, 6-1 Kasuga koen, Kasuga-shi, Fukuoka 816-8580, Japan*

† Electronic supplementary information (ESI) available: XAFS spectra. See DOI: https://doi.org/10.1039/d3ra08641k

sample) to improve its conductivity; particularly, Li_2FeS_2 has been reported to show a relatively high electronic conductivity and a high Li^+-diffusion coefficient,[18] the coexistence of which would be advantageous for improving the rate capability of Li_8FeS_5.

Experimental

The Li_8FeS_5-MM sample was prepared by mechanical milling technique; a blended powder of Li_2S and FeS in a 4 : 1 molar ratio was mechanically milled (MM) for 5–40 h using a planetary ball mill apparatus (Fritsch Pulverisette 7) under a rotating speed of 400 rpm to yield Li_8FeS_5-MM (5–40 h) samples. The previously reported Li_8FeS_5-H with a rather homogeneous component was also prepared by heating (600 °C) and subsequent milling for 40 h, for comparison.[13] Since Li_2S and the resulting Li_8FeS_5 are very sensitive to atmospheric moisture, all the procedures except for the heating and mechanical milling were carried out in an argon-filled glove box; the heating and mechanical milling were carried out under atmospheric conditions using an argon-filled container and a pot wherein Li_2S and Li_8FeS_5 were enclosed. We also prepared the Li_8FeS_5–Li_2FeS_2 composite by mechanically milling the blended powder of the above-mentioned Li_8FeS_5-MM (40 h) and Li_2FeS_2 in a 6 : 4 weight ratio for 1 h (Li_2FeS_2 was prepared by heating Li_2S and FeS in a 1 : 1 molar ratio at 1000 °C).

The phase purity of the sample was checked using X-ray diffraction (XRD) measurements (RINT TTR-III, Rigaku, Japan) using a monochromatic Cu Kα radiation within the 2θ range of 10–80°. Before the measurements, each sample was covered with a Kapton film in an argon-filled glove box, and the measurements were carried out within 1 h to minimize the reaction with atmospheric moisture. Structural refinement by X-ray Rietveld analysis was carried out using the RIETAN-2000 program.[19] The microstructure of the sample was examined using a high-resolution TEM (Talos F200X, ThermoFisher Scientific) operating at 300 kV in scanning mode with a probe current of 300 pA. The valence state and local structure of S atoms for the sample powders were examined by S K-edge X-ray absorption fine structure (XAFS) measurements, which were carried out at the soft X-ray double crystal monochromator beamline, BL-10, of the Synchrotron Radiation Center, Ritsumeikan University.[20] The total electron yield (TEY) method was used, and the incident X-ray beam was monochromatized with a Ge (111) crystal ($2d$ = 6.532 Å) pair. The photon energy was calibrated with the strong resonance of K_2SO_4 (S 1s → t2) appearing at 2481.7 eV.[21] All samples were sealed in an argon-filled transfer vessel.[20]

The electrical conductivity of each sample was measured using an electrochemical test device (Celltest 1470E, Solartron Analytical) with applied voltages of 50, 100, and 150 mV, after the sample powder was cold-pressed into a pellet with a diameter of 10 mm and thickness of 0.7 mm. The all-solid-state cells (10 mm in diameter) were assembled using the above-mentioned Li_8FeS_5-MM or Li_8FeS_5–Li_2FeS_2 by uniaxial pressing in the same manner as described previously.[17] Argyrodite-type sulfide solid electrolyte (SE) powder (80 mg) was pelletized and the positive electrode powder (5 mg), which was prepared by blending Li_8FeS_5-MM (or Li_8FeS_5–Li_2FeS_2), SE, and acetylene black (AB) in a 4 : 5 : 1 weight ratio, was loaded on the above-mentioned SE pellet, which were then pressed together under 360 MPa for 5 min into a laminated pellet. After an indium foil (9 mm diameter and 0.3 mm thick) and a lithium foil (8 mm diameter and 0.2 mm thick) were attached on the opposite side as a negative electrode, it was pressed under 90 MPa for 2 min. The unit cell element was then fastened using stainless steel rods and sealed into a solid-state cell. The electrochemical measurements were carried out at 25 °C initially with charging, after standing for 1 h on open circuit, using a TOSCAT-3100 instrument (Toyo System, Japan) at a current density of 0.13 mA cm^{-2} (50 mA g^{-1}, corresponding to *ca.* 0.1 C) when charging, and those of 0.13, 0.25, 0.64, and 1.3 mA cm^{-2} when discharging, between 3.0 and 1.0 V. Cyclic voltammetry (CV) of the cell was also conducted in the voltage range of 1.0–3.0 V (*vs.* Li–In) using a potentiostat/galvanostat (Model 1400, Solartron Analytical) at scan rates of 0.1 and 0.5 mV s^{-1}.

Results and discussion

The obtained Li_8FeS_5-MM powders were greyish-black in appearance, and their XRD patterns are shown in Fig. 1(a). With increasing milling time, the initial crystalline Li_2S and FeS changed to low-crystallinity Li_2S and FeS, and finally, XRD peaks originating from FeS were not detected; the XRD pattern of Li_8FeS_5-MM (40 h) was very similar to that of the previous Li_8FeS_5-H sample. The FeS content, estimated by X-ray Rietveld analysis and listed in Table 1, decreased with milling time, accompanied by a slight decrease in the lattice parameter of Li_2S. This indicates the decomposition of FeS and the partial substitution of smaller Fe^{2+} ions (0.66 Å) for Li^+ ions (0.74 Å)[22] in Li_2S *via* the milling process. Therefore, the milling process decreases the crystallite size of initial Li_2S and FeS, promoting the mutual chemical reaction (in particular, the incorporation of Fe^{2+} ions in Li_2S) and resulting in finally forming low-crystallinity rather homogeneous Fe-substituted Li_2S. The measured electrical conductivity of the Li_8FeS_5-MM samples was in the range of *ca.* 5×10^{-5}–8×10^{-5} S cm^{-1}, as listed in Table 1, which was higher than that of the Li_8FeS_5-H sample (*ca.* 1.0×10^{-5} S cm^{-1}), probably due to the coexistence of small amounts of FeS (*ca.* 10^1 S cm^{-1})[23] and the incorporation of Fe^{2+} ions into Li_2S.

Fig. 1(b) shows the charge and discharge curves of the InLi/Li_8FeS_5-MM sample cells at different current densities. Data for the InLi/Li_8FeS_5-H sample cell are also shown for comparison. All the sample cells showed discharge plateaus at *ca.* 1.5 V, which corresponded to that at *ca.* 2.1 V in the previously reported Li/Li_8FeS_5-H sample cells with a non-aqueous liquid electrolyte.[13] The Li_8FeS_5-MM sample cells showed a higher discharge capacity, particularly at a higher current density, than that of the Li_8FeS_5-H sample cell. The specific discharge capacity at a lower current density (0.13 mA cm^{-2}) for the Li_8FeS_5-MM (20 h) sample cell (*ca.* 660 mA h g^{-1}) was comparable to that of the previously reported Li_8FeS_5-H sample cell (*ca.* 730 mA h g^{-1}) with a non-aqueous liquid electrolyte.[13] In

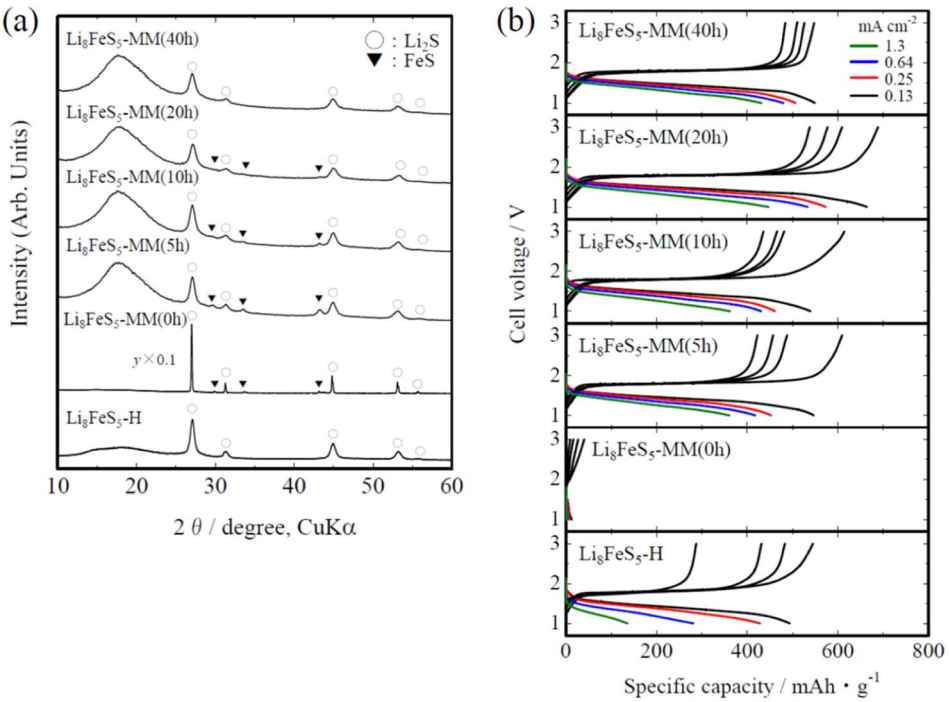

Fig. 1 (a) XRD patterns (Cu Kα radiation) and (b) charge and discharge profiles for the Li_8FeS_5-MM (0–40 h) sample cells at different current densities in the range of 0.13–1.3 mA cm^{-2} (50–500 mA g^{-1}, corresponding to *ca.* 0.1–1 C). Data for the Li_8FeS_5-H sample cell are also shown for comparison.

Table 1 FeS content (mol%) and lattice parameter (*a*/Å) of Li_2S estimated by X-ray Rietveld analyses for the Li_8FeS_5-MM and Li_8FeS_5–Li_2FeS_2 composite samples. The measured electrical conductivity values (σ/S cm^{-1}) are also listed. Data for the previous Li_8FeS_5-H sample are also listed for comparison[13]

	FeS content/mol%	*a*/Å	σ/S cm^{-1}
Li_8FeS_5-MM (0 h)	4(1)	5.71112 (9)	$<10^{-8}$
Li_8FeS_5-MM (5 h)	8(1)	5.710 (7)	5.0×10^{-5}
Li_8FeS_5-MM (10 h)	4(1)	5.709 (7)	5.8×10^{-5}
Li_8FeS_5-MM (20 h)	3(1)	5.704 (8)	8.4×10^{-5}
Li_8FeS_5-MM (40 h)	0(1)	5.704 (6)	7.4×10^{-5}
Li_8FeS_5–Li_2FeS_2	6(1)	5.711 (3)	4.4×10^{-4}
Li_8FeS_5-H[13]	0(1)	5.7048 (10)	1.0×10^{-5}

addition, the discharge capacity at higher current densities (*ca.* 450 mA h g^{-1} at 1.3 mA cm^{-2} for Li_8FeS_5-MM (20 h)) was comparable or superior to the previously reported values for all-solid-state Li–S batteries.[14–17]

Thus, the coexistence of the conductive component (FeS) in Li_8FeS_5 was effective for improving the rate capability of the all-solid-state cell. We then intended to introduce another conductive component, Li_2FeS_2, to obtain the Li_8FeS_5–Li_2FeS_2 composite; Li_2FeS_2 additives would be advantageous for improving both the electronic conductivity and Li^+ diffusion in the composite.[17] Fig. 2(a) shows the XRD pattern of the obtained Li_8FeS_5–Li_2FeS_2 composite. As in the above-mentioned Li_8FeS_5-MM samples, the Li_8FeS_5–Li_2FeS_2 composite consisted of low-crystallinity Li_2S and small amounts of FeS. No XRD peaks originating from Li_2FeS_2 were detected, probably due to its decomposition and conversion to FeS as well as its incorporation into Li_2S (resulting in Fe-substituted Li_2S) *via* the milling process. The FeS content and the lattice parameter of Li_2S, estimated by the X-ray Rietveld analysis, are also listed in Table 1; judging from the data, the Li_8FeS_5–Li_2FeS_2 composite seems very similar to the Li_8FeS_5-MM (5–10 h) samples. Fig. 2(b) shows the charge and discharge curves of the Li_8FeS_5–Li_2FeS_2 sample cells at different current densities. Even at a higher current density, the cell showed high discharge capacity compared with the Li_8FeS_5-MM sample cells (Fig. 1(b)). Such improved rate capability is evident from the capacity retention, as shown in Fig. 2(c). CV measurements also showed consistent results; as shown in Fig. 2(d), the Li_8FeS_5-H sample cell showed a reductive peak at *ca.* 1.4 V under 0.1 mV s^{-1} but not obvious at a higher scan rate (0.5 mV s^{-1}), whereas the Li_8FeS_5–Li_2FeS_2 sample cell showed an evident peak even under a higher scan rate. The measured electrical conductivity of the Li_8FeS_5–Li_2FeS_2 composite was *ca.* 4.4×10^{-4} S cm^{-1}, higher than that of the Li_8FeS_5-MM samples (*ca.* 5–8 $\times 10^{-5}$ S cm^{-1}). Such higher conductivity is responsible for the improved rate capability in the Li_8FeS_5–Li_2FeS_2 sample cell. In addition, the Li_8FeS_5–Li_2FeS_2 sample cell showed improved cycle performance, as shown in Fig. 2(e) and (f), partly due to its higher conductivity; higher conductivity could improve the utilization of the active materials as well as suppress the localized charging inhomogeneity. Because the XRD results showed similar estimated FeS contents and lattice parameters of Li_2S for the Li_8FeS_5–Li_2FeS_2 and Li_8FeS_5-MM (5–10 h) samples (Table 1), there would be some characteristic microstructures that cause the difference in

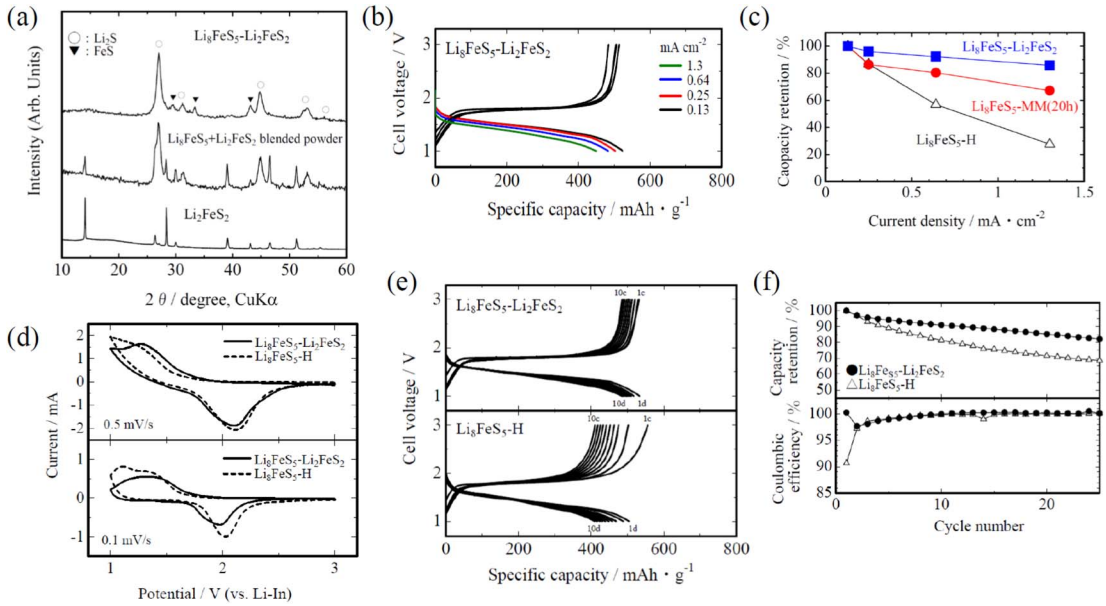

Fig. 2 (a) XRD patterns (Cu Kα radiation) of the Li_2FeS_2, Li_8FeS_5 + Li_2FeS_2 blended powder, and Li_8FeS_5–Li_2FeS_2 composite samples. (b) Charge and discharge profiles of the Li_8FeS_5–Li_2FeS_2 sample cell at different current densities in the range of 0.13–1.3 mA cm^{-2} (50–500 mA g^{-1}, corresponding to *ca.* 0.1–1 C). (c) Capacity retention at different current densities for the Li_8FeS_5-H, Li_8FeS_5-MM (20 h), and Li_8FeS_5–Li_2FeS_2 sample cells. (d) CV profiles at 0.1 and 0.5 mV s^{-1}, (e) charge and discharge profiles (10 cycles), and (f) capacity retention and coulombic efficiency of the Li_8FeS_5–Li_2FeS_2 and Li_8FeS_5-H sample cells at a current density of 0.13 mA cm^{-2}.

the XAFS measurements and TEM observations for the Li_8FeS_5–Li_2FeS_2 sample.

Fig. S1† shows the S K-edge X-ray absorption near-edge structure (XANES) spectra of the Li_8FeS_5–Li_2FeS_2 and Li_8FeS_5-H samples. Both samples showed similar spectra with three characteristic absorption peaks at 2469 eV (assigned to the bound state resonance due to an electronic transition between the S 1s and p-hybridized Fe 3d bands), 2472–2473 eV (originating from the 1s → 3p electronic transition in sulphur atoms), and 2476 eV (originating from the electronic transition of the 1s electron in S^{2-} to the unoccupied orbital with S 3p and Li 2s characters).[13,24] These spectral similarities indicate that the valence state and local structure around the S atoms are nearly consistent among these samples; that is, the Fe, Li, and S atoms surrounding the S atoms coordinate in a similar configuration on average while including slight fluctuations individually.

In contrast to the XAFS results, TEM observations showed a characteristic microstructure in the Li_8FeS_5–Li_2FeS_2 sample. As

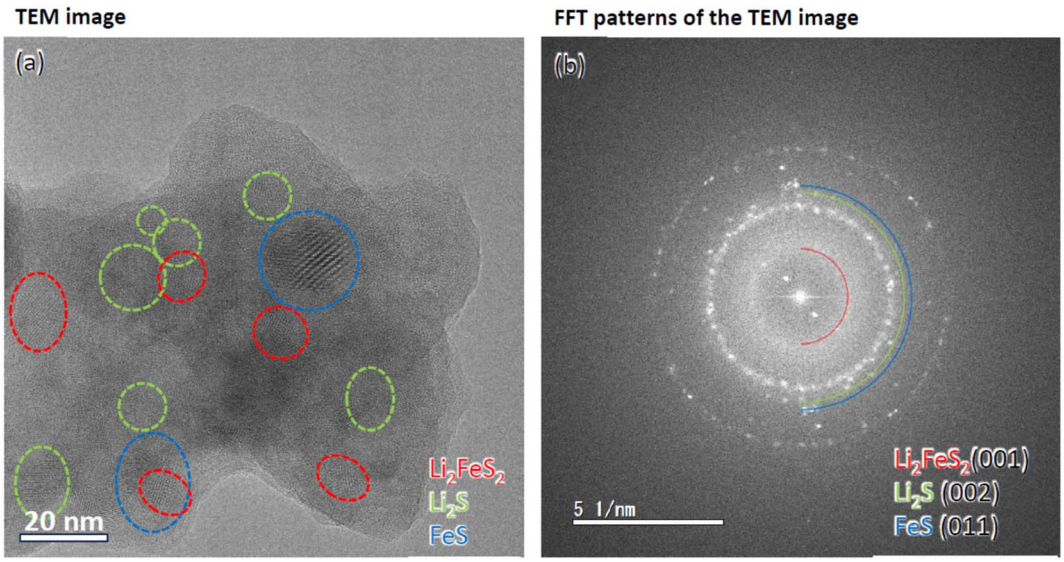

Fig. 3 (a) High-resolution TEM image and (b) fast Fourier transform (FFT) patterns of the TEM image for the Li_8FeS_5–Li_2FeS_2 sample. Several semicircles corresponding to the Debye–Scherrer rings originating from Li_2FeS_2(001), Li_2S(002), and FeS(011) are shown as examples.

shown in Fig. 3(a), the high-resolution TEM images showed the presence of some lattice fringes with domain sizes of *ca.* 10–20 nm distributed randomly in the amorphous (non-crystalline) background in the Li_8FeS_5–Li_2FeS_2 sample. In order to confirm the structure of each lattice fringe, the fast Fourier transform (FFT) pattern (pseudo diffraction pattern) of the TEM image was obtained (Fig. 3(b)), where several Debye–Scherrer rings and a halo pattern were observed. By careful comparison of the lattice spacings with previously reported crystallographic data,[25] they were assigned to the Li_2S and FeS components (for example, *ca.* 0.29 nm for Li_2S(002) and *ca.* 0.27 nm for FeS(011)). A notable point is that the extra component, not assigned to Li_2S and FeS, remained, and it was assigned to Li_2FeS_2 (for example, *ca.* 0.63 nm for Li_2FeS_2(001)). Although no peaks ascribed to Li_2FeS_2 were detected in the XRD pattern (Fig. 2(a)), there remained very small (or close to amorphous) Li_2FeS_2 crystallites in the Li_8FeS_5–Li_2FeS_2 sample. By inverse Fourier transformation of the FFT pattern, the locations of these three components (Li_2S, FeS, and Li_2FeS_2) were approximately identified in the TEM image and denoted in Fig. 3(a). Such a microstructure would be responsible for the higher conductivity and improved rate capability of the all-solid-state cell. Particularly, the difference in rate capability between the Li_8FeS_5-MM and Li_8FeS_5–Li_2FeS_2 sample cells (Fig. 2(c)) would originate from the coexistence of small crystallites of Li_2FeS_2 having higher Li^+ diffusion. In addition, the difference between the Li_8FeS_5-MM (40 h) and Li_8FeS_5-H sample cells (Fig. 1(b)) (both samples showed no FeS content estimated in XRD) might be due to the coexistence of small crystallites of FeS in the Li_8FeS_5-MM (40 h) sample; the higher conductivity of the Li_8FeS_5-MM (40 h) sample indicates the coexistence of small crystallites of FeS (XRD is usually detectable for a crystallite of size more than 10 nm). Thus, designing a microstructure, in which small crystallites of high conductive and high Li^+ diffusion components coexist, is effective for assembling all-solid-state cells with improved rate capability.

Conclusions

A Fe- and Li-containing polysulfide positive electrode material (Li_8FeS_5–Li_2FeS_2 composite) was successfully prepared, and it showed a high specific capacity (>500 mA h g^{-1}) with improved rate capability in all-solid-state cells. XRD results showed that this composite consisted of low-crystallinity Li_2S and FeS, whereas high-resolution TEM analysis indicated the coexistence of small crystallites of Li_2S, FeS, and Li_2FeS_2. This microstructure, in which highly conductive and high Li^+ diffusion components coexist, resulted in higher electrical conductivity and improved rate capability in all-solid-state cells.

Conflicts of interest

There are no conflicts to declare.

Acknowledgements

This work is based on the results obtained from a project, SOLiD-EV (JPNP18003), subsidized by the New Energy and Industrial Technology Development Organization (NEDO).

References

1 X. Ji and L. F. Nazar, *J. Mater. Chem.*, 2010, **20**, 9821–9826.
2 P. G. Bruce, S. A. Freunberger, L. J. Hardwick and J.-M. Tarascon, *Nat. Mater.*, 2012, **11**, 19–29.
3 Y.-X. Yu, *J. Phys. Chem. C*, 2019, **123**, 205–213.
4 J.-H. Li, J. Wu and Y.-X. Yu, *J. Mater. Chem. A*, 2021, **9**, 10186.
5 P. Das and P. Sarkar, *Phys. Chem. Chem. Phys.*, 2023, **25**, 30536.
6 K. A. J. Dilshad and M. K. Rabinal, *Phys. Chem. Chem. Phys.*, 2023, **25**, 11566.
7 M. N. Obrovac and J. R. Dahn, *Electrochem. Solid-State Lett.*, 2002, **5**, A70–A73.
8 A. Hayashi, R. Ohtsubo, T. Ohtomo, F. Mizuno and M. Tatsumisago, *J. Power Sources*, 2008, **183**, 422–426.
9 T. Shigedomi, Y. Fujita, T. Kishi, K. Motohashi, H. Tsukasaki, H. Nakajima, S. Mori, M. Tatsumisago, A. Sakuda and A. Hayashi, *Chem. Mater.*, 2022, **34**, 9745–9752.
10 M. Nagao, A. Hayashi and M. Tatsumisago, *J. Mater. Chem.*, 2012, **22**, 10015–10020.
11 T. Takeuchi, H. Kageyama, K. Nakanishi, M. Tabuchi, H. Sakaebe, T. Ohta, H. Senoh, T. Sakai and K. Tatsumi, *J. Electrochem. Soc.*, 2010, **157**, A1196–A1201.
12 K. Han, J. Shen, C. M. Hayner, H. Ye, M. C. Kung and H. H. Kung, *J. Power Sources*, 2014, **251**, 331–337.
13 T. Takeuchi, H. Kageyama, K. Nakanishi, M. Ogawa, T. Ohta, A. Sakuda, H. Sakaebe, H. Kobayashi and Z. Ogumi, *J. Electrochem. Soc.*, 2015, **162**, A1745–A1750.
14 A. Sakuda, T. Takeuchi, M. Shikano, H. Sakaebe and H. Kobayashi, *Front. Energy Res.*, 2016, **4**, 1–7.
15 A. Sakuda, T. Takeuchi, K. Okamura, H. Kobayashi, H. Sakaebe, K. Tatsumi and Z. Ogumi, *Sci. Rep.*, 2014, **4**, 4883.
16 Y. Kawasaki, H. Tsukasaki, T. Ayama, S. Mori, M. Deguchi, M. Tatsumisago, A. Sakuda and A. Hayashi, *ACS Appl. Energy Mater.*, 2021, **4**, 20–24.
17 M. Otoyama, T. Takeuchi, N. Taguchi, K. Kuratani and H. Sakaebe, *ECS Adv.*, 2023, **2**, 010501.
18 C. D. Wei, H. T. Xue, X. D. Zhao and F. L. Tang, *Phys. Chem. Chem. Phys.*, 2023, **25**, 8515–8523.
19 F. Izumi and T. Ikeda, *Mater. Sci. Forum*, 2000, **321**, 198–203.
20 K. Nakanishi, S. Yagi and T. Ohta, *AIP Conf. Proc.*, 2010, **1234**, 931.
21 M. Kiguchi, T. Yokoyama, D. Matsumura, H. Kondoh, T. Ohta and Y. Kitajima, *Phys. Rev. B: Condens. Matter Mater. Phys.*, 1999, **60**, 16205–16210.
22 R. D. Shannon, *Structure and Bonding in Crystals*, Academic Press. Inc., 1981, vol. ii, pp. 53–70.
23 H. Kobayashi, N. Takeshita, N. Mori, H. Takahashi and T. Kamimura, *Phys. Rev. B: Condens. Matter Mater. Phys.*, 2001, **63**, 115203.
24 S. Bodeur and J. M. Esteva, *Chem. Phys.*, 1985, **100**, 415–427.
25 ICSD (Inorganic Crystal Structure Database) code 68380 (Li2FeS2), 168079 (FeS), and 409397 (Li2S).